Clays and Clay Minerals, Vol. 55, No. 4, 354–360, 2007.

Eu INCORPORATION BEHAVIOR OF A Mg-Al-Cl LAYERED DOUBLE HYDROXIDE

HILDE CURTIUS* AND KRISTIAN UFER

Institute of Energy Research (IEF), IEF-6: Safety Research and Reactor Technology, Forschungszentrum Jülich GmbH, D-52425 Jülich, Germany

Abstract—From leaching experiments with metallic uranium-aluminum research reactor fuel elements in repository-relevant $MgCl_2$-rich salt brines, a Mg-Al layered double hydroxide (LDH) with chloride as the interlayer anion was identified as a crystalline secondary phase component. The incorporation behavior of europium into the structure of the Mg-Al-Cl LDH was investigated. Synthesis *via* co-precipitation was performed. The Mg-Al-Eu-Cl LDH obtained was treated with a concentrated ammonium carbonate solution. No release of Eu was detected; hence the molar stoichiometry of the LDH remained stable with respect to Mg, Al and Eu. This chemical behavior might be the first indication of the incorporation of Eu.

The material was further examined by powder X-ray diffraction. Structural parameters were obtained from comparisons of simulated and experimental diffraction patterns of a CO_3^{2-}-exchanged Mg-Al-Eu LDH and a Mg-Al LDH. The two materials showed different behaviors according to stacking order and lattice parameters. This is an indirect indication of the incorporation of Eu.

Key Words—Europium, Fuel Elements, Incorporation, LDH, Secondary Phases, Stacking Faults.

INTRODUCTION

Due to the political decision that there should be no reprocessing of research reactor fuel elements in Germany, the direct disposal of spent fuel elements has to be investigated. A possible repository for the spent fuel elements is a salt mine, and the accident scenario for long-term safety analysis is a hypothetical water ingress. Different leaching experiments with material test reactor fuel elements (MTR-FE) in highly concentrated salt brines at 90ºC showed that the radionuclides were rapidly mobilized, but then trapped by the corrosion products (Brücher *et al.*, 2001). (The MTR-FE of the DIDO type contains 20 wt.% U-Al alloy with an initial enrichment of 80% in ^{235}U. The fuel alloy plates, which are 0.6 mm thick, are covered on both sides with aluminum claddings of 0.38 mm, making the total thickness 1.36 mm. The spent fuel elements will be disposed of in a cast iron POLLUX container.) Investigations (Mazeina *et al.*, 2003) of these secondary corrosion products as a near-field barrier against radionuclide migration indicated that one component is a Mg-Al-Cl LDH, also referred to as a hydrotalcite-like compound (HTlc).

The LDHs can be structurally characterized as brucite-like sheets in which some divalent cations have been substituted by trivalent ions to form positively charged sheets. The cationic charge created in the sheets is compensated by the presence of anions in the interlayer (Miyata, 1975). In the free space in this interlayer, water molecules are also present. The main features of LDH structures and of LDH properties are determined by the nature of the brucite-like sheet, by the type of stacking of the brucite-like sheets, by the amount of water and by the position and type of anions in the interlayer. Bookin and Drits (1993) derived all possible polytypes of one-, two-, three- and six-layer stackings. These polytypes can be classified by the resulting interlayer polyhedra. These interlayer polyhedra form either octahedral coordination spheres (O-type) or trigonal prismatic spheres (P-type) for the interlayer anions. CO_3^{2-}-intercalated LDH prefer P-type arrangements which allow hydrogen bonding of the carbonate oxygen to the hydroxyls of the brucitic sheet. Only two polytypes fulfill this condition of forming only prismatic polyhedra. One is the trigonal $3R_1$ polytype with rhombohedral symmetry and the other is the hexagonal $2H_1$ polytype.

In the $3R_1$ form, adjacent layers are translated by a stacking vector (2/3,1/3,1/3) relative to each other (Figure 1a). The $2H_1$ polytype is formed by an alternate stacking of layers which are rotated around 180º parallel to the adjacent layers (Figure 1b). The interlayer anions occupy the six-fold prismatic polyhedra. Along the *z* direction, these anions are located at the center of the interlayer space. In the case of CO_3^{2-} the triangle lies parallel to the *ab* plane and the oxygen ions point in the direction of the octahedral hydroxyls to form hydrogen bonds with the hydroxyls of the brucitic sheet. Cl^--intercalated LDH also occupy at least partly the P position, but show a more disordered interlayer arrangement (Hou *et al*., 2002). The difference in the two P-type polytypes is the arrangement of the octahedral cations between two layers. Both stacking forms can occur in the same crystallite, so that the two

* E-mail address of corresponding author:
h.curtius@fz-juelich.de
DOI: 10.1346/CCMN.2007.0550403

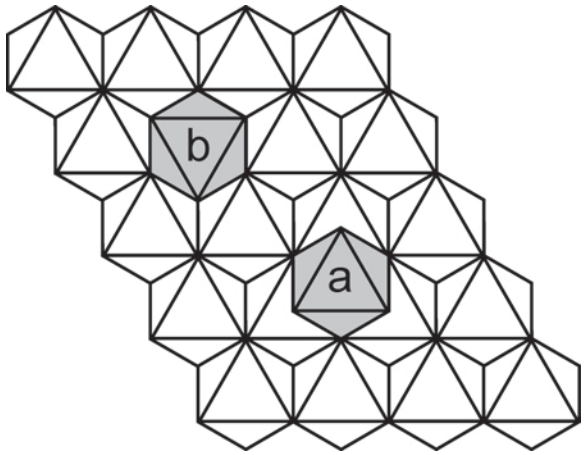

Figure 1. Projection in the *ab* plane for the two different P-type stackings. The upper layer is only represented by a single octahedron (gray). (a) $3R_1$ stacking; (b) $2H_1$ stacking.

polytypes are end-members of various sequences of the two stacking arrangements (Radha *et al.*, 2005).

Because of the need for safe long-term disposal, the prediction of radionuclide migration in the environment is of great importance. Mobilization of radionuclides and their release into the biosphere, due to corrosion processes caused by the fuel containment and the fuel itself, cannot be allowed. Therefore the prediction of radionuclide migration requires detailed understanding of the processes that control the interaction of metal ions with minerals and rocks. The corrosion products (secondary phases) can be viewed as a first barrier with respect to radionuclide mobilization. Among the controlling processes are surface complexation, ion exchange and co-precipitation, the last of these being of special interest. Ionic exchange and surface complexation are reversible processes. Co-precipitation, on the other hand, leads to an incorporation of the element in the structure and is an irreversible process. A remobilization of the element is only possible when a change in the chemical conditions is so significant that the host component itself dissolves.

In the present paper the incorporation behavior of Eu was studied. We chose the element Eu-III as a chemical analog for trivalent actinides.

EXPERIMENTAL

Synthesis of the Mg-Al-Eu LDH

Deionized water was boiled and stored under an argon atmosphere before use.

Chemicals were purchased from Merck and Aldrich and used without further treatment. All experiments were performed under an argon atmosphere.

The Mg-Al-Eu-Cl LDH was obtained according to the following co-precipitation process: 250 mL of water were placed in a three-necked glass flask and a pH of 10 was achieved using 2 M NaOH. A mixed aqueous solution of $MgCl_2 \cdot 6H_2O$ (0.3 M), $AlCl_3 \cdot 6H_2O$ (0.09 M) and $EuCl_3 \cdot 6H_2O$ (0.01 M) in 250 mL of water was added over a period of 3 h while the pH was maintained at 10 by addition of 2 M NaOH. The temperature was maintained at 70ºC. After the addition was complete, the temperature was raised to 90ºC and stirring was continued for 24 h. After cooling to room temperature, the precipitate formed was filtered and then dialyzed at 60ºC. For dialysis, a dialysis hose was filled with the substance and placed in a 2 L vessel containing deionized water. The water was changed continually until it was chloride-free (chloride measurements were performed with the cuvette test LCK 311, Dr Lange). The precipitate was filtered and dried in a desiccator.

Chemical analysis

The substance obtained was characterized by photometry, differential thermal analysis-thermogravimetric analysis (DTA-TGA), Fourier transform infrared (FTIR), inductively coupled plasma-optical emission spectroscopy (ICP-OES) and X-ray diffraction (XRD). For DTA-TGA, XRD and FTIR measurements, dry samples were milled to powder. For photometric and inductively couple plasma-mass spectrometry (ICP-MS) measurements the solid samples were dissolved in 2 M HNO_3. Furthermore, 1 g of the synthesized Mg-Al-Eu-Cl LDH was treated with 40 mL of an ammonium carbonate solution (0.5 mol/L) at room temperature for 24 h. Then the solid was separated by filtration, washed with 10 mL of water and dried at 70ºC. To determine the Mg, Al and Eu molar ratios of the solid, an ICP-OES analysis was performed as follows: 100 mg of the solid were dissolved in 10 mL of 1 M nitric acid. This solution was diluted (1 to 1000) with a 0.1 M nitric acid solution and the measurement performed.

To obtain detailed information about the incorporation of Eu, investigations by XRD and time-resolved laser fluorescence spectroscopy (TRLFS) were performed.

Table 1. Atom positions for a brucitic layer.

Atom	*x*	*y*	*z*	Occ.
Layer 1				
Mg	0	0	1.008 Å	0.750
Al	0	0	1.008 Å	0.225
Eu	0	0	1.008 Å	0.025
O	1/3	2/3	2.016 Å	1
O	2/3	1/3	0.000 Å	1
Layer 2				
Mg	0	0	1.008 Å	0.750
Al	0	0	1.008 Å	0.225
Eu	0	0	1.008 Å	0.025
O	1/3	2/3	0.000 Å	1
O	2/3	1/3	2.016 Å	1

Table 2. Parameters for simulation of XRD patterns.

Parameter	Variation range	Fixed value
a (Å)	3.05−3.11	3.065
Stacking order $3R_1$:$2H_1$	100:0−0:100	50:50
Random stacking (%)	0−50	0
Disk radius (Å)	30−150	100
Substitution Al−Eu	$Al_{1.0}Eu_{0.0}$−$Al_{0.0}Eu_{1.0}$	$Al_{0.9}Eu_{0.1}$
Distance C−O (Å)	1.10−1.35	1.29
Interlayer water per formula unit	0.0 H_2O−4.8 H_2O	0.0 H_2O

X-ray diffraction

The XRD data were collected with a Bruker D8 Advance™ diffractometer. The diffractometer with Bragg-Brentano geometry was equipped with a Cu tube, an automatic divergence slit (6 mm sample length) and a position-sensitive detector (Vantec™) with an active length of 3º. The patterns were recorded from 8º to 130º2θ with a step width of 0.007º2θ and a total measuring time of 5 h. To check the correct peak positions, additional measurements with an internal standard (ZnO) were performed. As a comparison for the XRD investigation, a Eu-free Mg-Al-Cl LDH was prepared and measured using the same conditions. For the Mg-Al-Eu-Cl LDH it was necessary to subtract reflections of an $Eu(OH)_3$ impurity. The relative intensities of these peaks were calculated from an $Eu(OH)_3$ structural model (Mullica *et al*., 1979). The Rietveld method (Rietveld, 1967) was used to quantify the amount of $Eu(OH)_3$. For that measurement, a known proportion of ZnO was used so that the LDH diffraction line could be viewed as a strong modulated background using the DDM method (Solovyov, 2004). The refinement was performed using the program BGMN (Bergmann *et al*., 1998).

Structural interpretations were limited to the CO_3^{2-} forms of the LDHs. The carbonate-intercalated LDHs are more stable during XRD analysis thereby avoiding the problem of mixed interlayer occupations or changes during measurement.

The main motivation for the XRD simulations was to ascertain whether the differences in the powder patterns of the Mg-Al LDH and the Mg-Al-Eu LDH can be explained by the incorporation of Eu and to verify that this incorporation leads to a structural change.

Simulations of powder patterns are widely used to obtain structural information from disordered LDHs (*e.g.* Radha *et al*., 2005; Thomas *et al*., 2004; Drits and Bookin, 2001). In this work, we calculated XRD patterns according to the method of Drits and Tchoubar (1990), using a computer program by Plançon (2002). The

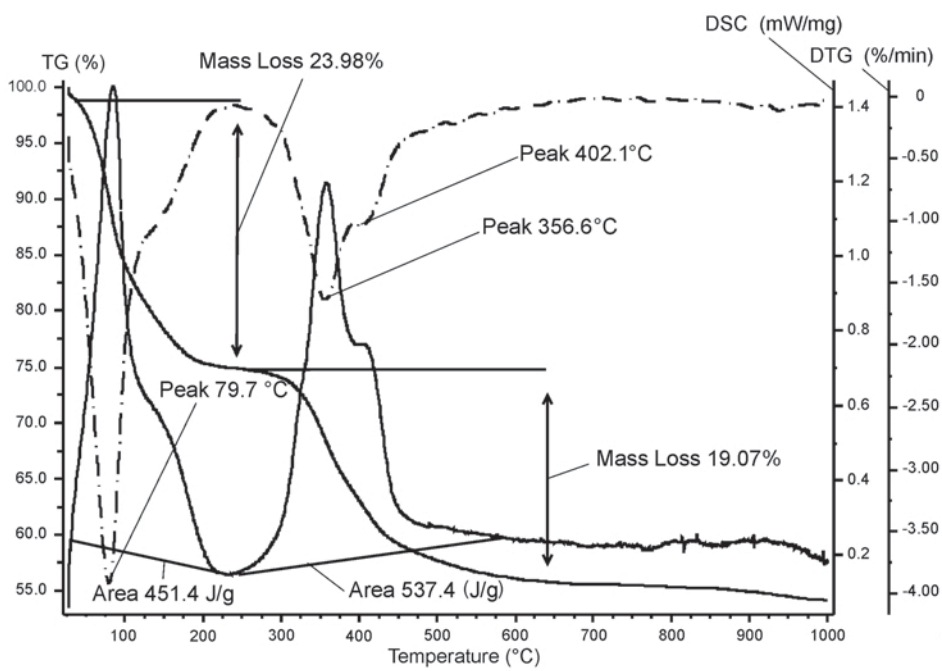

Figure 2. DTA-TGA thermogram of the Mg-Al-Eu-Cl LDH.

simulated patterns were compared to measured patterns by a semi-manual trial and error procedure.

The simulations were performed in the range 32−90º2θ. This range contains reflections of the *hk* reflection classes 10, 11 and 20. The structural parameters were chosen to be as simple as possible. Table 1 lists the atom positions for the brucitic sheets for a unit-cell with a = 3.605 Å. The z coordinates are given in absolute values (Å). The introduction of layer 2 was necessary to realize $2H_1$ stacking. No distortion of the octahedra was assumed and the interlayer occupation was considered as mono-ionic. Along the z direction the CO_3^{2-} was placed in the center of the interlayer parallel to the brucitic sheet. The oxygen ions point in the direction of the octahedral hydroxyls. $3R_1$ stacking was implemented by a stacking vector (2/3,1/3,C) for layer 1 to layer 1 and (1/3,2/3,C) for layer 2 to layer 2. For the $2H_1$ stacking (layer 1 to layer 2 and layer 2 to layer 1) a vector (0,0,C) was used, C being the layer thickness, derived from the basal reflections. In addition to the $3R_1$ and the $2H_1$ stacking, only different portions of random stackings were taken into consideration. The additional interlayer water was introduced by increasing the occupation of the carbonate oxygen. Table 2 lists the parameters which were varied to fit the experimental diffraction line. Only one parameter was varied at a time while the others were kept fixed. The range of variations and the fixed value are also given in Table 2. A user-defined background was added to the calculated patterns. The complete calculated pattern was automatically scaled to the experimental pattern by a least-squares minimization of the difference of the two patterns. This residual was also used to judge the simulation and to find the best fit.

RESULTS AND DISCUSSION

The Mg-Al-Eu-Cl LDH was prepared according to the co-precipitation method of Weiss and Toth (1996). Small modifications were made to the process, *e.g.* in the purification and drying steps. For the synthesized LDH, a Mg/Al/Eu mole ratio of 3:0.94:0.099 was determined by ICP-OES. In the DTA-TGA thermogram (Figure 2), the first endothermic peak between room temperature and 250ºC with its maxima at 79.7ºC, corresponding to a weight loss of 23.98%, is due to desorption of the interlayer water. The second endothermic peak between 250ºC and 500ºC indicates partial dehydroxylation in the main layer and elimination of chloride and carbonate in the interlayer.

The IR spectra show strong hydroxyl and water-stretching and -bending bands at 3467 and 1631 cm^{-1}. Al-O and Mg-O vibration bands appear in the region 1090 to 550 cm^{-1}. A very weak adsorption band due to adsorbed CO_3^{2-} was present at 1383 cm^{-1} (Figure 3).

From these results, the formula of the Mg-Al-Eu-Cl LDH can be derived as
$[Mg_3Al_{0.94}Eu_{0.099}(OH)_8]Cl_{0.95}(CO_3^{2-})_{0.03}5.71{\cdot}H_2O$.

For the solid, a specific surface area of 70 m^2/g was determined by BET and a cationic exchange capacity of 82 mmol/100 g was obtained by a complexation reaction with Cu-II-triethylentetraamin.

Furthermore, the treatment of the Mg-Al-Eu-Cl LDH with an ammonium carbonate solution as described by Duff *et al*. (2002) did not result in any change in the Mg-Al-Eu molar ratios, indicating that it is mainly Eu which is incorporated.

X-ray diffraction measurements were performed on a Mg-Al-Eu LDH and a Mg-Al LDH, both intercalated with Cl^- and with CO_3^{2-}. The diffraction patterns of the Cl^- form and the CO_3^{2-}-form are very similar except for the 00*l* reflections which vary in their position according to the different interlayer spacing of the two different forms. This confirms the observation of Allmann and Donnay (1969) that a Cl^--intercalated LDH is isostructural with a CO_3^{2-}-intercalated one. Figure 4 shows the patterns of Mg-Al-Eu-CO_3 LDH and Mg-Al-CO_3 LDH.

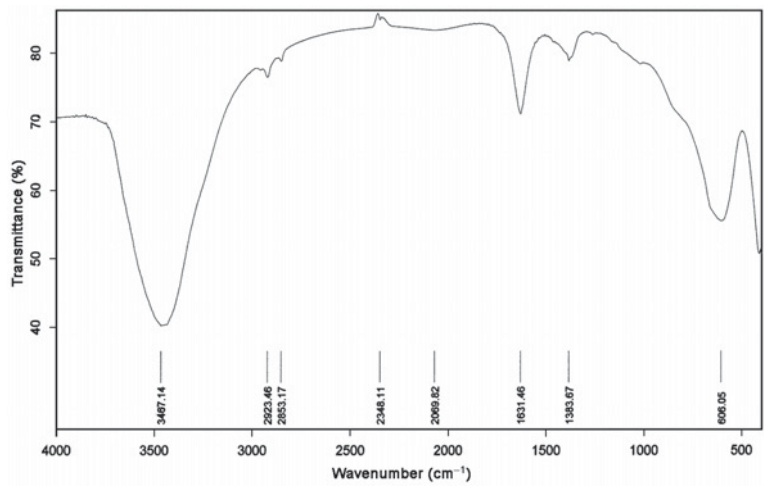

Figure 3. IR spectrum of the Mg-Al-Eu-Cl LDH.

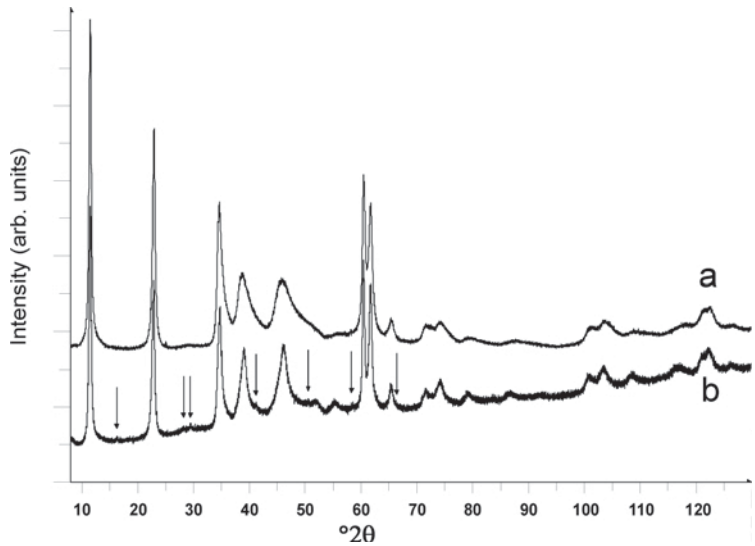

Figure 4. XRD pattern of the Mg-Al-CO_3 LDH (a) and the Mg-Al-Eu-CO_3 LDH (b). Peaks from an $Eu(OH)_3$ impurity in pattern b are marked with arrows. Cu radiation.

In the Eu LDH, the $Eu(OH)_3$ peaks are still present. For comparison with simulated patterns, these reflections were subtracted. Estimation of the $Eu(OH)_3$ impurity content with an internal standard showed that the amount of $Eu(OH)_3$ is of the order of <0.3 wt.%.

Besides the symmetric 00*l* peaks we see very broad and asymmetric reflections, especially in the range 32−59º2θ which corresponds to the 10 class. These reflections cannot be indexed by either the $3R_1$ or the $2H_1$ polytype. The shape of the reflections for the Mg-Al-Eu LDH are slightly more symmetric than for the Mg-Al LDH. In addition two small humps appear in the Mg-Al-Eu LDH pattern at 52º2θ and at 55º2θ.

Between 59 and 63º2θ are two sharp and symmetric reflections which belong to the 11 class. In the range above 63º2θ we see only broad modulations of the diffraction line. In this region we would expect the 20 reflection class. A comparison with patterns calculated by Drits and Bookin (2001) shows that the measured patterns correspond to a pattern of a defective stacking of the two polytypes. For a more detailed comparison we compared the measured patterns to >70 calculated patterns. The examination of these calculated patterns showed that different regions of the diffraction line are sensitive in different ways to the varied parameters. Table 3 summarizes qualitatively the different effects of the parameters on the patterns. Several parameters have an influence on the intensity of the reflections, *e.g.* the atomic content of a unit-cell, the substitution of Al by Eu, or the distance from C to O in the carbonate group and the interlayer water. Unfortunately the amount of interlayer water is the dominant effect and this is strongly superimposed on the Al-Eu substitution. For that reason, it is not possible to prove the presence of Eu directly from the XRD pattern. For the best fit, the ratio of Al:Eu was kept fixed by the initial weight, assuming that all Eu is located in the octahedral positions of the brucitic sheets. The variations of the lattice constant, *a*, showed that this is the only effect which has a significant influence on the position of the reflections. The first of the two reflections between 59 and 63º2θ can be indexed as 110 for both polytypes. Due to its sharpness it can be used to calculate *a* directly by $a = 2 \cdot d_{110}$.

The shapes of the reflections of the 10 and the 20 class are dominated by the stacking order. The differences for the 10 class, in particular, can be explained by different ratios of $3R_1$ and $2H_1$ stackings and different amounts of additional random stacking.

Table 3. Influence of the parameters on the XRD patterns.

Region	32−59º2θ	59−63º2θ	63−90º2θ
a	Weak (position)	Weak (position)	Weak (position)
Stacking order: $3R_1$:$2H_1$	Strong (shape)	No influence	Strong (shape)
Stacking order: random	Weak (int.+shape)	Weak (int.+shape)	Weak (int.+shape)
Disk radius	Weak (shape)	Strong (shape)	Weak (shape)
Substitution Al-Eu	Weak (intensity)	Weak (intensity)	Weak (intensity)
Distance C-O	Weak (intensity)	Weak (intensity)	Weak (intensity)
Interlayer water	Strong (intensity)	Strong (intensity)	Strong (intensity)

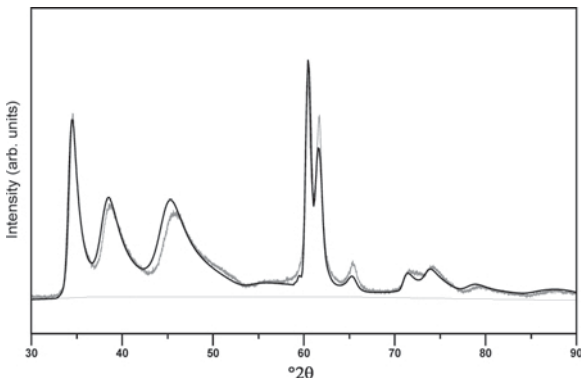

Figure 5. Best fit of the Mg-Al-CO_3 LDH. Bold black line – calculated pattern; gray line – measured pattern; thin black line – background. Cu radiation.

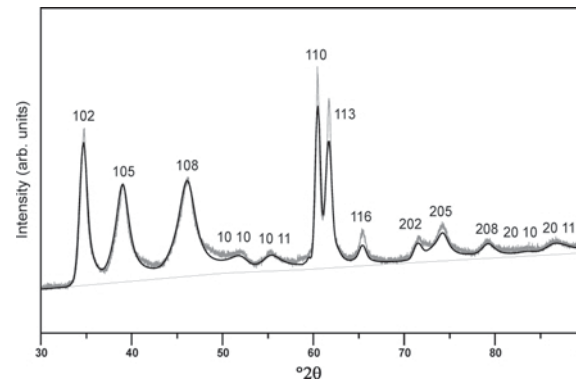

Figure 6. Best fit of the Mg-Al-Eu-CO_3 LDH. Bold black line – calculated pattern; gray line – measured pattern; thin black line – background. Cu radiation.

The results of the optimized fits are shown in Figures 5 and 6 and the resulting parameters in Table 4. The increase in the lattice parameter *a* of the Mg-Al-Eu-CO_3 LDH compared with that of the Mg-Al-CO_3 LDH is small but significantly improves the fit of the calculated and the experimental patterns. This change can be explained by the incorporation of Eu in the lattice. The stacking order of the Mg-Al-Eu LDH is much greater than for the Mg-Al LDH. It shows a clear favoritism of the $3R_1$ polytype (71%) while the Mg-Al LDH is a mixture of equal proportions of $3R_1$ and $2H_1$ stacking. In addition, the Mg-Al-Eu LDH shows a much smaller portion of random stacking. The peaks of the Mg-Al-Eu LDH were indexed following the metric of the pure $3R_1$ polytype. For the Mg-Al LDH, indexing was omitted because of the lack of preference for one polytype. The two additional maxima between 50 and 57°2θ can be regarded as a pre-stage of the 10 10 and the 10 11 reflections of a pure $3R_1$ stacking.

The increased ordering of the stacking can be interpreted as a result of different long-range interactions between the cations in adjacent layers, induced by the exchange of Al by Eu.

Although we reached a good agreement between the observed and calculated patterns there are still misfits. The results shown in this work are the best fits which can be achieved with the limited choice of parameters we considered here. By introducing more parameters, *e.g.* additional stacking vectors or mixed interlayer anion occupations, better agreement may be possible. We have shown that certain differences in the patterns can definitely be ascribed to structural features which indicate the incorporation of Eu in the octahedral sheet of the LDH. This is in agreement with TRLFS measurements from Stumpf *et al*. (2007). It was shown that the Eu^{3+} ion was incorporated by the LDH lattice and surrounded by six hydroxyl groups.

CONCLUSION

From previous results it was shown that a non-irradiated metallic U/Al-Al fuel element corroded completely in a Mg-rich salt brine and a Mg-Al-Cl LDH was identified as a crystalline phase component in the corrosion products. The present investigations were performed in order to study the incorporation behavior of repository-relevant radionuclides into the lattice of this LDH and therefore synthesis of a Mg-Al-Eu-Cl LDH was performed. From the analytical data the formula of the Mg-Al-Eu-Cl LDH was derived as $[Mg_3Al_{0.94}Eu_{0.099}(OH)_8]Cl_{0.95}(CO_3^2)^-_{0.03}5.71{\cdot}H_2O$. The first indications of successful incorporation of Eu were obtained by reactions with an ammonium carbonate solution. The molar ratio of Mg-Al-Eu did not change.

Table 4. Parameters for the best fit of the XRD patterns.

Parameter	Mg-Al LDH	Mg-Al-Eu LDH
a (Å)	3.061	3.063
Stacking order $3R_1$:$2H_1$	50:50	71:29
Random stacking (%)	35	17
Disk radius (Å)	80	80
Substitution Al–Eu	–	0.9–0.1*
Distance C–O (Å)	1.25	1.25
Interlayer water per formula unit	1.50	1.38

* fixed by initial weight

From the XRD results, the differences noted in the pattern can definitely be ascribed to structural features which indicate the incorporation of Eu in the octahedral sheet in which the Eu is surrounded by six hydroxyl groups, as indicated by TRLFS measurements.

These results show that an irreversible immobilization of radionuclides by incorporation in the crystal lattice of the Mg-Al-Cl LDH is possible.

REFERENCES

Allmann, R. and Donnay, J.D.H. (1969) About the structure of iowaite. *American Mineralogist*, **54**, 296–298.

Bergmann, J., Friedel, P. and Kleeberg, R. (1998) BGMN – a new fundamental parameters based Rietveld program for laboratory X-ray sources, its use in quantitative analysis and structure investigations. *Commission of Powder Diffraction, International Union of Crystallography, CPD Newsletter*, **20**, 5–8.

Bookin, A.S. and Drits, V.A. (1993) Polytype diversity of the hydrotalcite-like minerals. I. Possible polytypes and their diffraction features. *Clays and Clay Minerals*, **41**, 551–557.

Brücher, H., Curtius, H. and Fachinger, J. (2001) R&D for Back-End options for irradiated research reactor fuel in Germany. *Transactions of the 5th Topical Meeting on Research Reactor Fuel Management*, April 1–3 2001, Aachen, Germany, ENS RRFM.

Drits, V.A. and Bookin, A.S. (2001) Crystal structure and X-ray identification of layered double hydroxides. Pp. 39–92 in: *Layered Double Hydroxides: Present and Future* (V. Rives, editor). Nova Science, New York.

Drits, V. A. and Tchoubar, C. (1990) *X-ray Diffraction by Disordered Lamellar Structures*. Springer Verlag, New York, 371 pp.

Duff, C.M., Coughlin, J.U. and Hunter D.G. (2002) Uranium co-precipitation with iron oxide minerals. *Geochimica et Cosmochimica Acta*, **66**, 3533–3547.

Hou, X., Kalinichev, A.G. and Kirkpatrick, R.J. (2002) Interlayer structure and dynamics of Cl^{-}-$LiAl_2$-layered double hydroxide: ^{35}Cl NMR observations and molecular dynamics modelling. *Chemistry of Materials*, **14**, 2078–2085.

Mazeina, L., Curtius, H., Fachinger, J. and Odoj, R. (2003) Characterisation of secondary products of uranium-aluminium material test reactor fuel element corrosion in repository-relevant brine. *Journal of Nuclear Material*, **323**, 1–7.

Miyata, S. (1975) The synthesis of hydrotalcite-like compounds and their structures and physico-chemical properties. *Clays and Clay Minerals*, **31**, 369–375.

Mullica, D.F., Milligan, W.O. and Beall, G.W. (1979) Crystal Structures of $Pr(OH)_3$, $Eu(OH)_3$ and $Tm(OH)_3$. *Journal of Inorganic and Nuclear Chemistry*, **41**, 525–532.

Plançon, A. (2002) CALCIPOW: a program for calculating the diffraction by disordered lamellar structures. *Journal of Applied Crystallography*, **35**, 377.

Radha, A.V., Shivakumara, C. and Kamath, P.V. (2005) DIFFaX simulations of stacking faults in layered double hydroxides (LDHs). *Clays and Clay Minerals*, **53**, 520–527.

Rietveld, H.M. (1967) Line profiles of neutron powder-diffraction peaks for structure refinement. *Acta Crystallographica*, **22**, 151–152.

Solovyov, L.A. (2004) Full-profile refinement by derivative difference minimization. *Journal of Appied Crystallography*, **37**, 743–749.

Stumpf, T., Curtius, H., Walther, C., Dardenne, K., Ufer, K. and Fanghänel, Th. (2007) Incorporation of Eu(III) into a hydrotalcite: a TRLFS and EXAFS study. *Environmental Science and Technology*, **41**, 3186–3191.

Thomas, G.S., Rajamathi, M. and Kamath, P.V. (2004) DiffaX simulations of polytypism and disorder in hydrotalcite. *Clays and Clay Minerals*, **52**, 693–699.

Weiss, A. and Toth, E. (1996) Untersuchungen zur Synthese, Quellungseigenschaften und Anionenaustausch von kristallchemisch modifizierten Doppelhydroxiden vom Hydrotalkit-Typ. *Jahrestagung der DTTG, Freiberg*, 267–276.

(*Received 19 September 2006; revised 16 April 2007; Ms. 1220; A.E. James E. Amonette*)